IJMMM International Journal of Minerals, Metallurgy and Materials 矿物冶金与材料学报（英文版）

Electrochemical properties of Ca–Pb electrode for calcium-based liquid metal batteries

Xiao-hui Ning, Chen-zheng Liao, and Guo-qing Li

Cite this article as:
Xiao-hui Ning, Chen-zheng Liao, and Guo-qing Li, Electrochemical properties of Ca–Pb electrode for calcium-based liquid metal batteries, *Int. J. Miner. Metall. Mater.*, 27(2020), No. 12, pp. 1723-1729. https://doi.org/10.1007/s12613-020-2150-9

Articles you may be interested in

Kai-lin Cheng, Dao-bin Mu, Bo-rong Wu, Lei Wang, Ying Jiang, and Rui Wang, Electrochemical performance of a nickel-rich $LiNi_{0.6}Co_{0.2}Mn_{0.2}O_2$ cathode material for lithium-ion batteries under different cut-off voltages, *Int. J. Miner. Metall. Mater.*, 24(2017), No. 3, pp. 342-351. https://doi.org/10.1007/s12613-017-1413-6

Yuan Li, Li-na Cheng, Wen-kang Miao, Chun-xiao Wang, De-zhi Kuang, and Shu-min Han, Nd–Mg–Ni alloy electrodes modified by reduced graphene oxide with improved electrochemical kinetics, *Int. J. Miner. Metall. Mater.*, 27(2020), No. 3, pp. 391-400. https://doi.org/10.1007/s12613-019-1880-z

Ying-zhong Ma, Chang-lin Yang, Yun-jin Liu, Fu-song Yuan, Shan-shan Liang, Hong-xiang Li, and Ji-shan Zhang, Microstructure, mechanical, and corrosion properties of extruded low-alloyed Mg–*x*Zn–0.2Ca alloys, *Int. J. Miner. Metall. Mater.*, 26(2019), No. 10, pp. 1274-1284. https://doi.org/10.1007/s12613-019-1860-3

Hong-xiang Li, Shi-kai Qin, Ying-zhong Ma, Jian Wang, Yun-jin Liu, and Ji-shan Zhang, Effects of Zn content on the microstructure and the mechanical and corrosion properties of as-cast low-alloyed Mg–Zn–Ca alloys, *Int. J. Miner. Metall. Mater.*, 25(2018), No. 7, pp. 800-809. https://doi.org/10.1007/s12613-018-1628-1

Levent Kartal and Servet Timur, Direct electrochemical reduction of copper sulfide in molten borax, *Int. J. Miner. Metall. Mater.*, 26(2019), No. 8, pp. 992-998. https://doi.org/10.1007/s12613-019-1821-x

Le-ping Wang, Gang Chen, Qi-xin Shen, Guo-min Li, Shi-you Guan, and Bing Li, Direct electrodeposition of ionic liquid-based template-free SnCo alloy nanowires as an anode for Li-ion batteries, *Int. J. Miner. Metall. Mater.*, 25(2018), No. 9, pp. 1027-1034. https://doi.org/10.1007/s12613-018-1653-0

IJMMM WeChat

QQ author group

International Journal of Minerals, Metallurgy and Materials
Volume 27, Number 12, December 2020, Page 1723
https://doi.org/10.1007/s12613-020-2150-9

Electrochemical properties of Ca–Pb electrode for calcium-based liquid metal batteries

Xiao-hui Ning, Chen-zheng Liao, and Guo-qing Li

Center for Advancing Materials Performance from the Nanoscale (CAMP-Nano), State Key Laboratory for Mechanical Behavior of Materials, Xi'an Jiaotong University, Xi'an 710049, China
(Received: 27 April 2020; revised: 17 July 2020; accepted: 20 July 2020)

Abstract: The Ca–Pb electrode couple is considered to be one of the least expensive (~36 $/(kW·h)) among various optional materials for liquid–metal batteries (LMBs). The electrochemical properties of Ca–Pb alloy in a Ca|LiCl–NaCl–$CaCl_2$|Pb cell were investigated in this paper. The electrode potential maintained a linear relationship in the current density range of 50–200 mA·cm^{-2}, which indicates that the alloying and dealloying processes of Ca with Pb attained rapid charge transfer and mass transport in the interface between the liquid electrode and electrolyte. The Ca–Pb electrode exhibited remarkable properties with a high discharge voltage of 0.6 V, a small self-discharge current density (<2 mA·cm^{-2} at 600°C), and a high coulombic efficiency (>98.84%). The postmortem analysis showed that intermetallics $CaPb_3$ and CaPb were uniformly distributed in the electrode with different molar fractions of Ca, which indicates that the nucleation of solid intermetallics did not hinder the diffusion of Ca in the electrode. This investigation on Ca–Pb electrode sheds light on the further research and the design of electrodes for Ca-based LMBs.

Keywords: liquid-metal battery; molten salt electrolyte; Ca–Pb alloys; electrochemical properties

1. Introduction

The liquid–metal batteries (LMBs) have attracted increasing attention for their grid storage application; they are considered as the promising electrochemical energy storage devices because of their long cycle life, low cost, and easy scale-up [1–2]. Different from other battery systems, LMBs have a unique three-liquid-layer structure composed of a liquid anode, an electrolyte, and a cathode. Given the density differences and immiscibility, the cell can self-segregate into three distinct layers at the operating temperature [3]. The anode and cathode are on the top and bottom respectively, and are electrically isolated by the molten salt electrolyte. Attributed by the three-liquid-layer structure design of the LMBs, the liquid/liquid interface causes the facile charge transfer and fast mass transport between the electrode and electrolyte [4–6]. Meanwhile, the molten salt electrolyte has a high electrical conductivity and thus a low ohmic loss [7–9]. The combination of the above two features enables the operation of LMBs at high charge–discharge rates, which is suitable for grid storage.

To date, the development of electrode systems for LMBs mainly focuses on the lithium-based system owing to the lowest electronegativity and solubility of lithium in its halide salts [10]. Li||Bi [3], Li||Bi–Sb [11], Li||Sb–Pb [12], Li||Sb–Sn [13], Li||Te–Sn [14], and Li||Sb–Bi–Sn [10] were intensively investigated. The results showed that the lithium-based LMBs delivered an average discharge voltage of 0.6–1.2 V and energy densities of 60–150 W·h·kg^{-1}. However, given the booming industry of lithium-ion battery, the restricted lithium supply for LMBs and the rapid price increase of lithium cannot be ignored.

Calcium is the fifth abundant element in the earth's crust, and it has a low standard reduction potential of –2.87 V vs. NHE (normal hydrogen electrode). These features make Ca a sustainable negative-electrode material for LMBs considering its application for large-scale energy storage. Fundamental studies have reported the thermodynamic and electrochemical properties of calcium-based LMB systems, such as Ca||Sb [15–16] and Ca||Bi [17–18]. They showed the competitive battery performance compared with lithium-based systems. However, in view of the cost of antimony and bismuth, Ca–Pb electrode couple is considered to have an excellent voltage (~0.6 V) and the lowest cost (~36 $/(kW·h))

Corresponding author: Xiao-hui Ning E-mail: xiaohuining@mail.xjtu.edu.cn

among various optional materials for Ca-based LMBs [2]. Meanwhile, Pb can also be alloyed with other elements to form Sb–Pb and Bi–Sb alloy positive electrodes; it can also contribute to the capacity beyond Sb and Bi. However, Ca has high solubility in its halide salts [19], which leads to the high self-discharge current in the Ca-based LMBs and therefore its low coulombic efficiency. The electrochemical properties of Ca–Pb in molten salt electrolyte are difficult to measure. Hence, Kim and his team [20] investigated the thermodynamic properties of Ca–Pb electrodes with CaF_2 solid electrolyte, which has proven its potential application in LMBs.

Herein, we employed a multi-cation molten salt (LiCl–NaCl–$CaCl_2$) as the electrolyte to suppress the solubility of Ca in molten salts. We proved the stability of the Ca–Pb system in a multi-cation electrolyte by measuring the electromotive force (emf) of the Ca–Pb electrode. Then, we investigated in detail the electrochemical properties of Pb as the positive electrode for potential application in LMBs and in the alloying–dealloying processes of Ca with Pb electrode.

The alloying and dealloying processes of Ca with Pb at the interface between the electrolyte and Pb electrode are illustrated as follows. During the alloying processes, Ca^{2+} is conducted through the electrolyte (mass transport), reduced, and then alloyed with Pb (charge transfer); Ca diffuses from the surface to the bulk of electrode (mass transport). The reverse of the processes occur when the Pb electrode is dealloyed.

The electrochemical cell in our study can be represented by the following formula:

$$\mathrm{Ca|LiCl-NaCl-CaCl_2|Pb} \quad (1)$$

where a multi-cation molten salt of LiCl–NaCl–$CaCl_2$ serves as the electrolyte with a molar ratio of 38.5:26.5:35.0 (melting temperature T_m = 457°C). The operating temperatures were set at 600 and 700°C in accordance with the Ca–Pb binary-phase diagram [21].

The potentials of the Ca–Pb electrode were calibrated to the value vs. pure Ca(s) by using the following equation:

$$E = E_{WE} - E_{ref} \quad (2)$$

where E_{WE} is the potential of the Ca–Pb working electrode (WE) vs. the Ca–Bi reference electrode (RE), and E_{ref} is the potential of the RE vs. pure Ca(s). At 600 and 700°C, the value of E_{ref} is 0.785 and 0.765 V, respectively [15].

2. Experimental

2.1. Material preparation

Pure Pb (99.999%, Alfa Aesar) was premelted in a boron nitride (BN) crucible (Saint-Gobain Advanced Ceramics) inside a glovebox with an inert argon atmosphere ($O_2 < 1 \times 10^{-7}$vol%, $H_2O < 1 \times 10^{-7}$vol%) and served as the WE. 0.15mol% Ca–Bi alloy was used as the counter electrode (CE) by melting pure Bi (99.999%, Alfa Aesar) and Ca (99.99%, Aldrich) in the BN crucible. The surface area of CE should be maintained and considerably larger than that of WE to provide facile transfer kinetics. 0.35mol% Ca–Bi alloy was adopted as the RE and was prepared in the same manner. The RE of 0.35mol% Ca–Bi alloy was a mixture of $Ca_{11}Bi_{10}$(s) and Bi(l), which is in the two-phase region, to ensure the stability of the RE potential. The potential of the alloy used as RE is fixed and does not change with the composition [22].

The high-purity anhydrous salts of LiCl (99.995%, Alfa Aesar), NaCl (99.99%, Alfa Aesar), and $CaCl_2$ (99.99%, Alfa Aesar) were used to prepare the LiCl–NaCl–$CaCl_2$ electrolyte with the molar ratio of 38.5:26.5:35.0. To obtain dry and homogenous electrolytes, we premelted the molten salt in a stainless crucible by the following procedures. (1) The electrolyte was placed in a heatable sealed container, evacuated to a pressure below 1 Pa, and heated to 80°C; the vacuum and temperature were maintained for 12 h. (2) Temperature was increased from 80 to 250°C, and the vacuum and temperature were maintained for 12 h. (3) The electrolyte was heated to 700°C and kept for 3 h under a flowing argon gas at 0.2 $cm^3 \cdot s^{-1}$. (4) The premelted electrolyte was ground into lumps measuring 5–10 mm in diameter in the glove box after cooling down to room temperature.

2.2. Electrochemical cell assembly

The three-electrode electrochemical cell was assembled in a glove box. During the induction melting process, the tungsten wires with a diameter of 1 mm (99.95%, Alfa Aesar) were inserted into each electrode to establish electrical contact. The wire was wrapped in an alumina tube (99.8%, McDanel Advanced Ceramic Technologies). The prepared three electrodes were arranged in an alumina crucible (99.8%, McDanel Advanced Ceramic Technologies). Then, the electrolyte was added to cover the electrodes. The electrochemical cell was placed in a stainless steel chamber. Fig. 1 shows the configuration of the experiment.

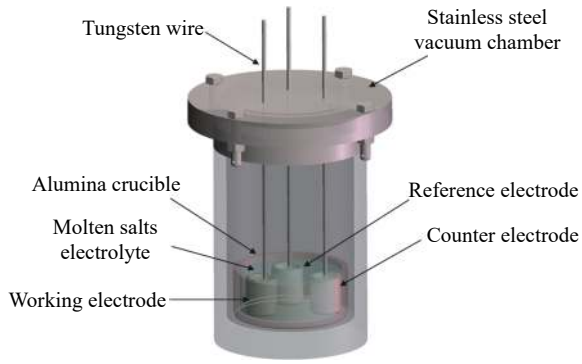

Fig. 1. Three-electrode electrochemical cell configuration, comprising the working electrode (WE), reference electrode (RE), and counter electrode (CE).

2.3. Electrochemical measurement

Electrochemical measurement was carried out with a potentiostat–galvanostat (PGSTAT302N) and a frequency response analyzer (FRA32M). The current density of 50 mA·cm^{-2} was used in the coulometric titration experiment. The dwelling time of the alloying and dealloying of Ca with Pb of each step was set to 3000 s, and the relaxation time of 5000 s was used to obtain the accurate equilibrium electrode potential (E_{eq}) after each step. The estimation of the molar fraction of Ca in WE (x_{Ca}) was assumed to be of 100% coulombic efficiency in this study. The potential of the WE was recorded at different current densities to assess the rate capability. Finally, the electrode potential of WE was held at 0.45 and 1.40 V for 12 h at 600 and 700°C, respectively, to obtain the self-discharge current of the cell. Furthermore, electrochemical impedance spectroscopy (EIS) was performed using a CHI660E electrochemical analyzer to accurately analyze the total resistance of the WE at the open circuit potential with a perturbation amplitude of 5 mV and a frequency range of 10 kHz to 0.01 Hz.

2.4. Postmortem analysis

The WEs at different alloying stages during the alloying process were quenched for postmortem analysis. The electrodes were examined by a stereomicroscope (Olympus SZ61) to observe the macroscopic morphology, whereas the microscopic morphology and composition were analyzed by scanning electron microscopy (SEM, JEOL6610) and energy dispersive X-ray spectrometry (EDS, IXRF System, Model 55i).

3. Results and discussion

3.1. Electromotive force measurement of Ca–Pb alloy in the molten salt electrolyte

The coulometric titration method was adopted to measure the equilibrium potential of Ca–Pb WE in the LiCl–NaCl–$CaCl_2$ molten salt electrolyte exactly. All measured results were compared with the data from the literature by using CaF_2 solid electrolyte to verify the reliability of the multi-cation molten salt electrolyte [20], because the CaF_2 was confirmed to have extremely low solubility of Ca metal in a previous study [23].

Fig. 2(a) shows the variation in the potential of Ca–Pb WE (E) and the current density (j) at 600°C. The equilibrium potential measured during the 12th and 13th dealloying steps were removed due to the drastic changes in the electrode potentials. The equilibrium potentials of Ca–Pb electrode at each molar fraction of Ca in the electrode were extracted from the value of the open circuit potential after each titration step. Figs. 2(b)–2(c) and Table 1 show the relationship of the equilibrium potentials of Ca–Pb electrode and the molar

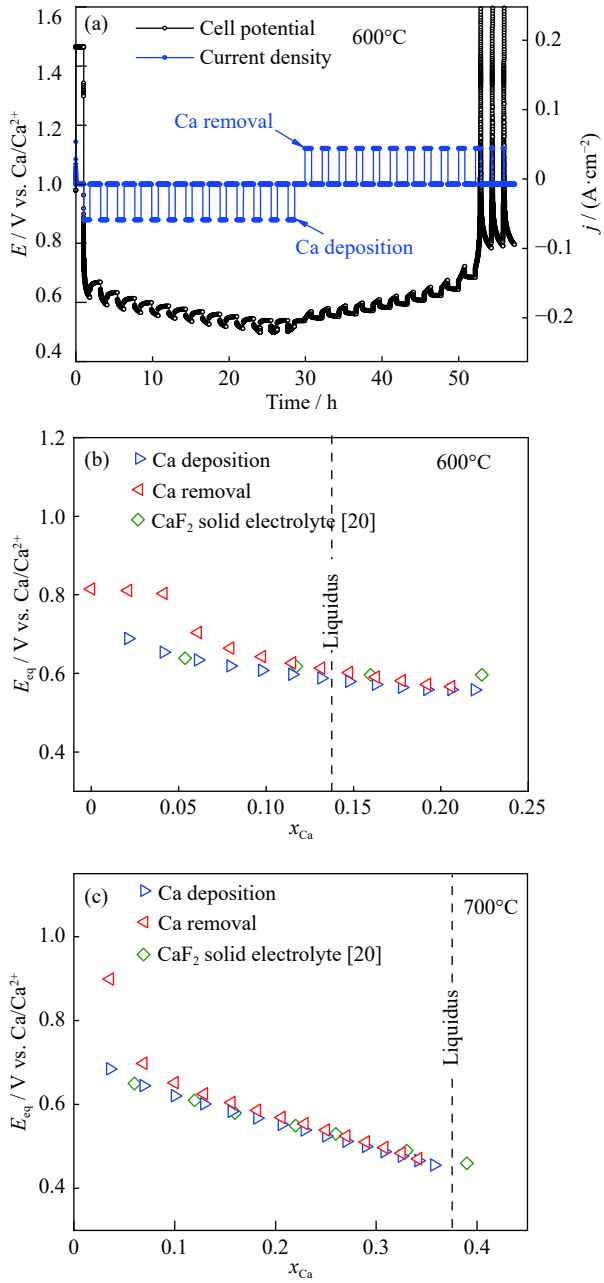

Fig. 2. (a) Variation of the potential of WE (E) and current density (j) during the coulometric titration measurement at 600°C; (b–c) equilibrium potential (E_{eq}) of the WE in LiCl–NaCl–$CaCl_2$ molten salt electrolyte measured as a function of molar fraction of Ca in Ca–Pb electrode (x_{Ca}) at 600°C (b) and 700°C (c).

fraction of Ca in the Ca–Pb electrode. The test was performed at two different temperatures because the depth of titration varies with temperature. By comparing the data from our study and those in the literature [20] (Fig. 2 and Table 1), we can conclude that the emf values measured by using the multi-cation molten salt as the electrolyte and that measured by using CaF_2 solid electrolyte were generally in good agreement (with difference of less than 3%). Thus, the multi-cation

molten salt electrolyte can effectively diminish the solution of Ca. The slight differences may arise from the existence of self-discharge current. As shown in Fig. 2(b), the emf values dropped firstly and stabilized after decreasing to 0.6 V, but the emf values continually dropped in the Fig. 2(c). This result was caused by the increase in the solubility of Ca in Pb with the increase temperature.

3.2. Kinetics of Ca–Pb alloying and dealloying

To evaluate the kinetics of Ca–Pb alloying and dealloying processes, we obtained the potential of Ca–Pb electrode at the current density range from 50 to 200 mA·cm^{-2} at 600 and 700°C. The corresponding results are shown in Fig. 3. The cut-off voltage of the electrode was set as the value where the potential changes dramatically in this test. Figs. 3(a) and 3(b) show that the electrodes exhibited highly chemically reversible electrode reaction. Thus, with the increase in current density, the overpotential of Ca–Pb electrode also increased. A low discharge capacity was observed at high current densities. The electrode potential consistently showed a sharp decrease near the end of the Ca–Pb alloying process. This event possibly resulted from the nucleation of solid Ca–Pb intermetallics at the interface of liquid electrode/electrolyte.

3.3. Electrochemical performances of Ca–Pb alloy

Coulombic efficiency is vital to the evaluation of the electrochemical properties of Ca||Pb cell. The coulombic efficiency of the Ca–Pb electrode at 600°C was estimated on the basis of the data from Fig. 3(a), and the corresponding results are shown in Table 2. The coulombic efficiency of the cell increased from 98.8% to 102.4% with the current density gradually increasing from 50 to 200 mA·cm^{-2}. The variation in coulombic efficiency at different current densities can be attributed to the high self-discharge current of Ca–Pb electrode, which resulted from the high dissolution of Ca in the molten salt. Meanwhile, the dissolution of the Ca–Pb electrode in the electrolyte during the alloying process caused the loss of capacity, resulting in the coulombic efficiency exceeding 100% in the following dealloying process.

To investigate the self-discharge current in Ca||Pb cell quantitatively, we held the electrode potential of WE between 0.45 and 1.40 V for 12 h. Fig. 4 shows the measured self-dis-

Table 1. Equilibrium potentials of Ca–Pb alloys from coulometric titration (this work) and previously reported emf values obtained using CaF_2 [20] V vs. Ca/Ca^{2+}

x_{Ca}	600°C		700°C	
	This work	Ref. [20]	This work	Ref. [20]
0.02	0.69	—	—	—
0.04	0.65	—	0.68	—
0.06	0.63	0.62	—	0.65
0.07	0.62	—	0.65	—
0.10	0.61	—	0.62	—
0.11	0.60	—	—	—
0.12	—	0.60	—	0.61
0.13	0.59	—	0.60	—
0.15	0.58	—	—	—
0.16	0.57	0.58	0.58	0.58
0.18	0.56	—	0.57	—
0.19	0.56	—	—	—
0.21	0.56	—	0.55	—
0.22	0.56	0.58	—	0.55
0.23	—	—	0.54	—
0.25	—	—	0.53	—
0.26	—	—	—	0.53
0.27	—	—	0.51	—
0.29	—	—	0.50	—
0.31	—	—	0.49	—
0.33	—	—	0.48	0.49
0.34	—	—	0.47	—
0.35	—	—	—	—
0.36	—	—	0.46	—
0.39	—	—	—	0.46
0.42	—	—	—	—

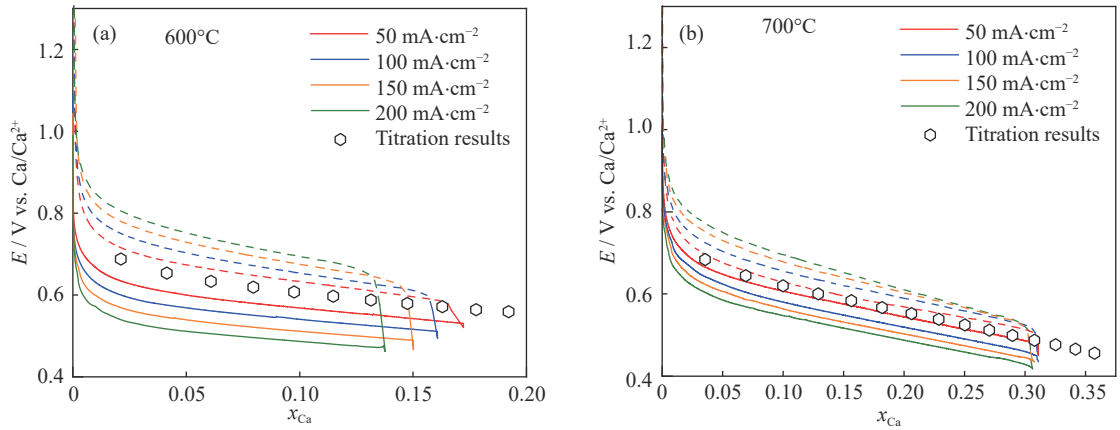

Fig. 3. Potential of the WE (E) measured as a function of molar fraction of Ca in Ca-Pb alloy (x_{Ca}) at different current densities during continuous alloying (solid lines) and dealloying (dotted lines) of Ca with the Pb electrode and the E_{eq} measured from titration results at (a) 600°C and (b) 700°C.

charge current of Ca–Pb electrode at 600°C and 700°C. The dealloying current flowed when the electrode potentials were greater than 0.7 V. This condition may be caused by the chemical transport of Ca into the Ca–Pb electrode with an electrode potential less than 0.7 V, that is, the alloying current flowed due to the dissolution of Ca–Pb alloy in the electrolyte [24]. However, when the electrode potential applied was close to 0.7 V, the self-discharge current density decreased to zero. The self-discharging current density for Ca–Pb was as low as 2 mA·cm^{-2} at 600°C compared with that at 700°C, which resulted in the high coulombic efficiency of the cell and ensured the accuracy of electrode potential measurement. This phenomenon may also prove that self-discharge current was mainly generated from the dissolution of Ca in the molten salt.

Table 2. Coulombic efficiency at different current densities at 600°C

Current density / (mA·cm^{-2})	Coulombic efficiency / %
50	98.84
100	99.27
150	100.00
200	102.42

The electrochemical impedance spectrum measurement was performed to understand the influence of charge transfer and mass transport on the electrochemical performance. Fig. 5(a) shows the Nyquist plots of Ca–Pb electrode at the open-circuit potentials at 700°C. The spectra formed a semi-circle at high frequencies and a straight line at low frequencies. The high-frequency semi-circle intercept represents the ohmic resistance R_{ohm}, and the semi-circle width denotes the charge transfer resistance R_{ct}. Table 3 tabulates the corresponding calculated impedance data of the charge transfer, ohmic, and mass transfer resistances.

In the typical three-electrode setup of our work, the ohmic resistance R_{ohm} was 0.06 Ω and was independent of the molar fraction of Ca in Ca–Pb alloy. However, the charge transfer resistance R_{ct} decreased substantially with the increase of Ca content from 0.30 to 0.22 Ω. This finding may be attributed to the formation of uniform Ca–Pb intermetallic compounds with the increased Ca content in the WE. Therefore, the thickness of liquid Pb decreased in the electrode, which resulted in the reduced diffusion distance of Ca to Ca–Pb electrode and thus facilitated the alloying process. The mass transport resistance R_{mt} can be calculated by subtracting R_{ohm} and R_{ct} from the total resistance R_t. The total resistance R_t was acquired based on the calculation of the slope of the line in Fig. 5(b). The corresponding results are shown in Table 3. The mass transport resistance R_{mt} showed minimal contribution to the total resistance. Thus, the charge transfer resistance R_{ct} plays a prominent role in the electrochemical process of the Ca–Pb alloying process.

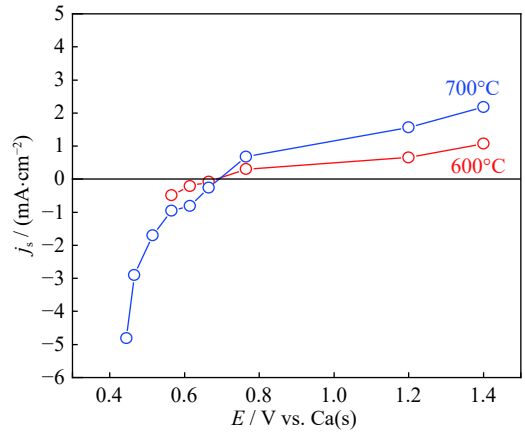

Fig. 4. Self-discharge current density j_s at different electrode potentials E at 600 and 700°C.

3.4. Postmortem analysis

We carried out postmortem analysis to investigate the microstructural evolution during the alloying process of Ca–Pb electrode. Three different samples with varying molar fractions of Ca were quenched to room temperature. All these

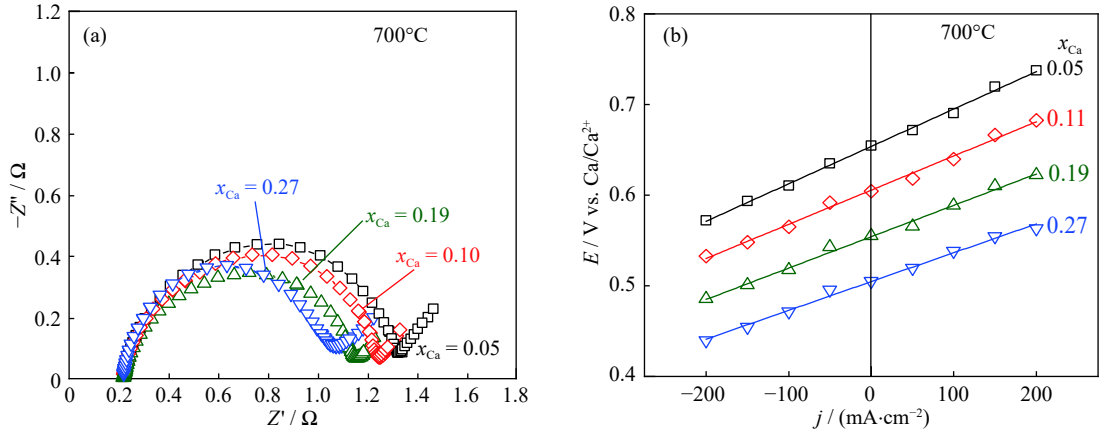

Fig. 5. (a) EIS obtained at the open-circuit potentials at 700°C; (b) potential of WE as a function of current density at 700°C.

Table 3. EIS data of Ca–Pb electrode at 700°C

x_{Ca}	R_t / Ω	R_{ohm} / Ω	R_{ct} / Ω	R_{mt} / Ω
0.05	0.41	0.06	0.30	0.05
0.11	0.38	0.06	0.28	0.04
0.19	0.35	0.06	0.26	0.03
0.27	0.32	0.06	0.22	0.04

Ca–Pb electrodes were prepared at 700°C with 200 mA·cm^{-2} current density. The molar fraction of Ca in these three electrodes was 0.05, 0.15, and 0.31, respectively. Fig. 6 shows the morphology of the electrodes and their composition. As shown in Fig. 6(a), the content of Ca in the WE was extremely low in the initial state of alloying. The electrode was mainly composed of Pb and contained a small amount of $CaPb_3$. As the content of Ca rose to x_{Ca} = 0.15, the content of $CaPb_3$ increased in the two-phase region in Fig. 6(b).

When the electrode was in the state of sharp potential drop (x_{Ca} = 0.31), a large amount of $CaPb_3$ was generated in the electrode, and a high-calcium intermetallic CaPb appeared at the top of the electrode (Fig. 6(c)). The nucleation of CaPb may be due to the highly concentrated region of Ca formed when the electrode passed a high current. The formation of these solid intermetallics greatly reduced the activity of Ca, resulting in a sudden decrease in electrode potential (Fig. 3(b)). In particular, the intermetallics $CaPb_3$ and CaPb did not accumulate at the interface between the electrode and the

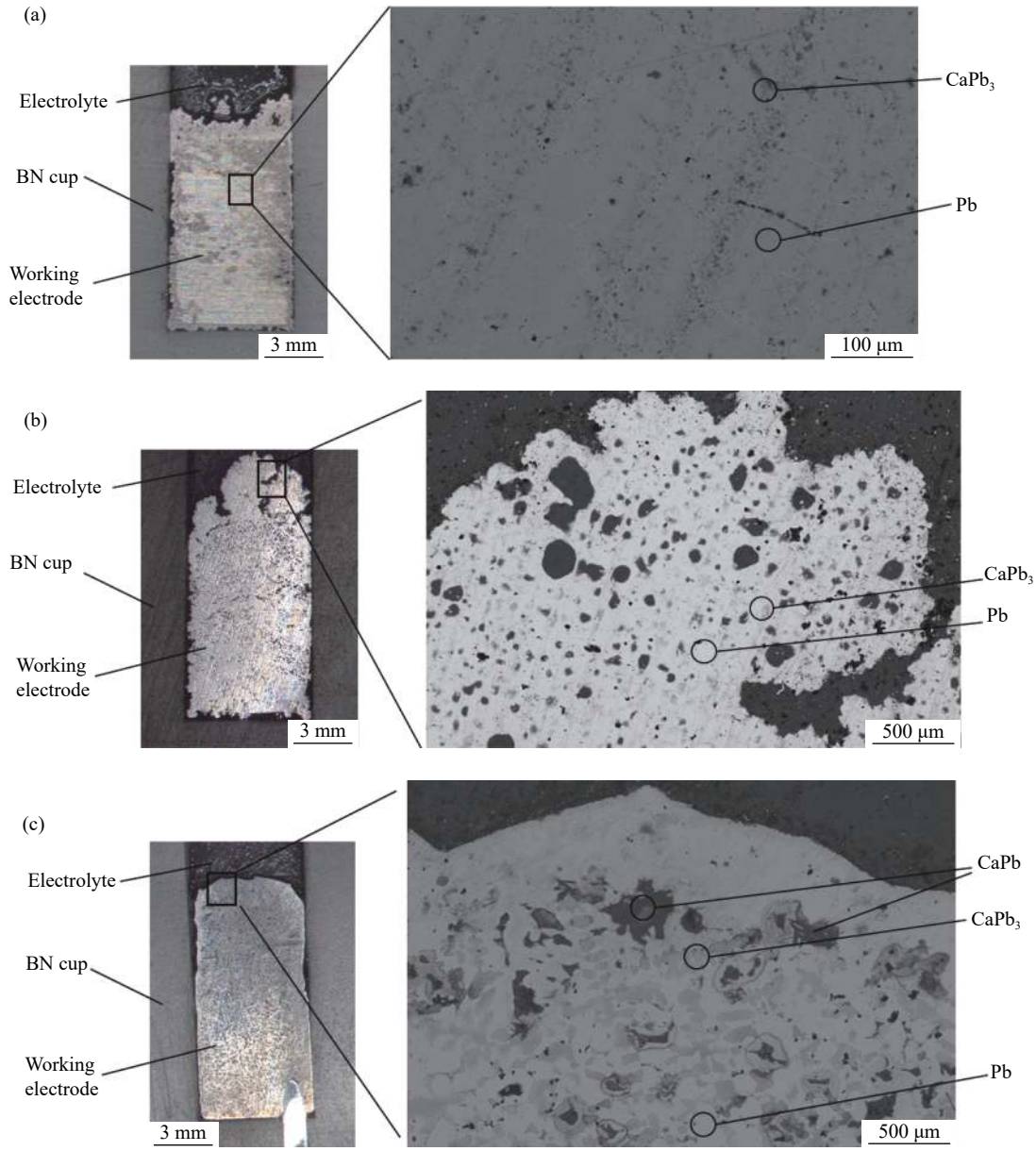

Fig. 6. Postmortem analysis of the WEs with different molar fractions of Ca at a current density of 200 mA·cm^{-2} at 700°C: (a) x_{Ca} = 0.05, (b) x_{Ca} = 0.15, and (c) x_{Ca} = 0.31.

electrolyte but were uniformly distributed in the electrode. This finding indicates that the nucleation of solid intermetallics in the electrode did not hinder the diffusion of Ca in the electrode and did not cause a large loss in the coulombic capacity of the battery, consistent with the results in Fig. 3(b).

4. Conclusion

The electrochemical properties of Ca–Pb as the positive electrode for LMB were evaluated in LiCl–NaCl–$CaCl_2$ molten salt. The solubility of Ca in the electrolyte was successfully suppressed by using the alloy electrode and a multication electrolyte. The electrode potential of Ca–Pb alloy and current density maintained a good linear relationship in the current density range of 50–200 $mA \cdot cm^{-2}$, and this finding confirms that the Ca–Pb electrode has excellent kinetics performance. The Ca–Pb positive electrode exhibited a high discharge voltage of 0.6 V and a high coulombic efficiency over 98.84%. Meanwhile, the cell showed a small self-discharge current density. Near the end of the Ca–Pb alloying process, a large amount of dispersed intermetallic $CaPb_3$ was found in the Ca–Pb electrode, which possibly resulted in a sudden drop in the electrode potential.

Acknowledgements

This work was financially supported by the National Key R&D Program of China (No. 2018YFB0905600), the National Natural Science Foundation of China (Nos. 51874228 and U1766216), and the Natural Science Foundation of Shaanxi Province, China (No. 2020JM-068).

References

[1] D.J. Bradwell, H.J. Kim, A.H.C. Sirk, and D.R. Sadoway, Magnesium-antimony liquid metal battery for stationary energy storage, *J. Am. Chem. Soc.*, 134(2012), No. 4, p. 1895.

[2] H.J. Kim, D.A. Boysen, J.M. Newhouse, B.L. Spatocco, B. Chung, P.J. Burke, D.J. Bradwell, J. Kai, A.A. Tomaszowska, K.L. Wang, W.F. Wei, L.A. Ortiz, S.A. Barriga, S.M. Poize-au, and D.R. Sadoway, Liquid metal batteries: Past, present, and future, *Chem. Rev.*, 113(2013), No. 3, p. 2075.

[3] X.H. Ning, S. Phadke, B. Chung, H.Y. Yin, P. Burke, and D.R. Sadoway, Self-healing Li-Bi liquid metal battery for grid-scale energy storage, *J. Power Sources*, 275(2015), p. 370.

[4] H.A. Laitinen, R.P. Tischer, and D.K. Roe, Exchange current measurements in KCl–LiCl eutectic melt, *J. Electrochem. Soc.*, 107(1960), No. 6, p. 546.

[5] A.D. Pasternak and D.R. Olander, Diffusion in liquid metals, *AIChE J.*, 13(1967), No. 6, p. 1052.

[6] G.J. Janz and N.P. Bansal, Molten salts data: Diffusion coefficients in single and multi-component salt systems, *J. Phys. Chem. Ref. Data*, 11(1982), No. 3, p. 505.

[7] L. Kartal and S. Timur, Direct electrochmical reduction of copper sulfide in molten borax, *Int. J. Miner. Metall. Mater.*, 26 (2019), No. 8, p. 992.

[8] S.Q. Jiao and H. Zhu, Novel metallurgical process for titanium production, *J. Mater. Res.*, 21(2006), No. 9, p. 2172.

[9] T. Dai, L. Yang, X.H. Ning, D.L. Zhang, R.L. Narayan, J. Li, and Z.W. Shan, A low-cost intermediate temperature Fe/Graphite battery for grid-scale energy storage, *Energy Storage Mater.*, 25(2020), p. 801.

[10] W. Zhao, P. Li, Z.W. Liu, D.L. He, K. Han, H.L. Zhao, and X.H. Qu, High-performance antimony-bismuth-tin positive electrode for liquid metal battery, *Chem. Mater.*, 30(2018), No. 24, p. 8739.

[11] T. Dai, Y. Zhao, X.H. Ning, R.L. Narayan, J. Li, and Z.W. Shan, Capacity extended bismuth-antimony cathode for high-performance liquid metal battery, *J. Power Sources*, 381(2018), p. 38.

[12] K.L. Wang, K. Jiang, B. Chung, T. Ouchi, P.J. Burke, D.A. Boysen, D.J. Bradwell, H.J. Kim, U. Muecke, and D.R. Sadoway, Lithium antimony-lead liquid metal battery for grid-level energy storage, *Nature*, 514(2014), No. 7522, p. 348.

[13] H.M. Li, K.L. Wang, S.J. Cheng, and K. Jiang, High performance liquid metal battery with environmentally friendly antimony-tin positive electrode, *ACS Appl. Mater. Interfaces*, 8(2016), No. 20, p. 12830.

[14] H.M. Li, K.L. Wang, H. Zhou, X.L. Guo, S.J. Cheng, and K. Jiang, Tellurium-tin based electrodes enabling liquid metal batteries for high specific energy storage applications, *Energy Storage Mater.*, 14(2018), p. 267.

[15] S. Poizeau, H.J. Kim, J.M. Newhouse, B.L. Spatocco, and D.R. Sadoway, Determination and modeling of the thermodynamic properties of liquid calcium-antimony alloys, *Electrochim. Acta*, 76(2012), p. 8.

[16] T. Ouchi, H.J. Kim, X.H. Ning, and D.R. Sadoway, Calcium-antimony alloys as electrodes for liquid metal batteries, *J. Electrochem. Soc.*, 161(2014), No. 12, p. A1898.

[17] H.J. Kim, D.A. Boysen, D.J. Bradwell, B. Chung, K. Jiang, A.A. Tomaszowska, K.L. Wang, W.F. Wei, and D.R. Sadoway, Thermodynamic properties of calcium-bismuth alloys determined by emf measurements, *Electrochim. Acta*, 60(2012), p. 154.

[18] H.J. Kim, D.A. Boysen, T. Ouchi, and D.R. Sadoway, Calcium-bismuth electrodes for large-scale energy storage (liquid metal batteries), *J. Power Sources*, 241(2013), p. 239.

[19] R.A. Sharma, The solubilities of calcium in liquid calcium chloride in equilibrium with calcium-copper alloys, *J. Phys. Chem.*, 74(1970), No. 22, p. 3896.

[20] N.D. Smith, N.E. Orabona, J.P.S. Palma, Y.R. Kong, C. Blanchard, and H.J. Kim, Thermodynamic properties of Ca–Pb electrodes determined by electromotive force measurements, *J. Power Sources*, 451(2020), art. No. 227745.

[21] M. Idbenalia, C. Servantb, N. Selhaouia, and L. Bouirdena, A thermodynamic reassessment of the Ca–Pb system, *Calphad*, 32(2008), No. 1, p. 64.

[22] C.J. Wen, B.A. Boukamp, R.A. Huggins, and W. Weppner, Thermodynamic and mass tra-nsport properties of "LiAl", *J. Electrochem. Soc.*, 126(1979), No. 12, p. 2258.

[23] A.S. Dworkin, H.R. Bronstein, and M.A. Bredig, The electrical conductivity of solutions of metals in their molten halides. VIII. Alkaline earth metal systems, *J. Phys. Chem.*, 70(1966), No. 7, p. 2384.

[24] M. Okada, R.A. Guidotti, and J.D. Corbett, Solution of sodium alloys of some post-tra-nsition metals in molten sodium halides. Evidence for anions of bismuth and antimony, *Inorg. Chem.*, 7(1968), No. 10, p. 2118.